Kinetics of domain growth, theory, and Monte Carlo simulations: A two-dimensional martensitic phase transition model system

Teresa Castán* and Per-Anker Lindgård
Physics Department, Risø National Laboratory, DK-4000 Roskilde, Denmark
(Received 15 March 1989)

By means of Monte Carlo computer simulation and scaling theory, we study the domain growth kinetics associated with a weak first-order transition between two non-symmetry-related ordered phases, exemplified by martensitic transformations, surface reconstructions, or magnetic transitions. The model studied has two kinds of domain walls: sharp, straight stacking faults, and broad, curved solitonlike walls. The domain wall motion after a deep quench to low temperature is found to follow the Allen-Cahn theory; nonetheless, the growth exponent for the excess energy $\Delta E(t) \sim t^{-n}$ has an exponent $n \sim \frac{1}{4}$, distinctly lower than the expected $n = \frac{1}{2}$, but in agreement with simulation results for some other models. A theoretical scaling analysis gives exactly $n = \frac{1}{4}$ and shows that the slow growth is a consequence of the fact that finite-size stacking faults cannot move until their extent is sufficiently small. The new universality class for domain growth is proposed as a singular Allen-Cahn class with $n = \frac{1}{4}$ for nonconserved order parameter, with domain walls of both exactly zero and finite curvature (whereas the domain-wall width or softness is not important as such). Since stacking faults and twin boundaries are common and have exactly zero curvature, we expect that many experimental systems belong to this class. The simulation results are also analyzed in terms of a soliton model as well as the Ginzburg-Landau theory; finally, a fast algorithm for domain growth studies is described.

I. INTRODUCTION

Many crystals, both metallic and insulating, which have a β-cubic (bcc) structure, undergo at low temperatures a structural phase transition to a closed-packed structure, in particular the hcp or fcc structures. This is called a martensitic transformation.[1] The low-temperature phase may consist of the simple $AB\cdots$ (hcp) or $ABC\cdots$ (fcc) stacking of closed-packed planes, or exhibit more complicated long periodic sequences, e.g., the $9R$ structure given by $\cdots ABA\,BCB\,CAC\cdots$. However, it often also exhibits random stacking faults or domain walls, which model random twin faults.[2] During the process of formation of the closed-packed phase, it breaks up into domains, which in the majority of cases are related to each other by the operation of twinning.[3] This is also found for the ordering process of solid solutions.[4] The theoretical description of these questions is often made using the one-dimensional axial next-nearest-neighbor Ising (ANNNI) model.[5] Another theoretical approach,[6] within the framework of strain-induced interaction theory, pioneered the use of Monte Carlo simulation of the kinetics of the martensitic transformation. Recently, a two-dimensional magnetic analog model with the martensitic transition symmetry has been developed[7] and the static behavior close to the transition point analyzed by computer simulations.

Here we are concerned with the dynamics of this model and, in particular, with the nucleation and growth of the domains of the low-temperature closed-packed phase, which takes place after a thermal quench to well below the phase-transition temperature. With the two-dimensional model it is possible to study the important interplay between the extent and the movement of the stacking faults, which is not possible in the one-dimensional models. Furthermore the model gives a fairly realistic description of the dynamics of the phase transition. The kinetics of domain growth by itself is a fundamental problem in a nonequilibrium statistical mechanics. The problem is also of practical interest in the fields of surface science,[8] metallurgy,[9] and earth sciences.[10]

When a system is quenched from a high-temperature disordered state to a state below the transition temperature, the ordered phase appears by the nucleation of p types of small ordered domains separated by walls of disorder, when the order parameter has a degeneracy p. As the time t after the quench increases, these domains coarsen and the unfavorable excess free energy due to the walls is reduced. In the late stages the domain sizes are much larger than all microscopic lengths, and in analogy with critical phenomena one expects a scaling behavior[11] and expects the growth law for the domain size $R(t)$ to have a power-law form $R(t) \propto t^n$, where n is some "universal" exponent. In case $R(t)$ is the only relevant length, the excess free energy must decrease with the same exponent $\Delta E(t) \sim t^{-n}$. The universal character means that many different systems exhibiting a wide variety of growth processes, fit into a few classes with different characteristic growth exponents. The number of classes and the characteristic physical features of these are currently under active debate. A main feature is established to be the character of the order parameter. If it is a nonconserved quantity, the Allen-Cahn theory[12] predicts that the domain growth process is driven by the lo-

cal curvature of the walls giving rise to a late-time behavior characterized by an exponent $n=\frac{1}{2}$. If instead the order parameter is conserved, the late-time behavior is expected to follow the Lifshitz-Slyozov law[13] with $n=\frac{1}{3}$; we will not consider this case here.

In several investigations of systems with nonconserved order parameter one has indeed found $n=\frac{1}{2}$. These include low-energy electron diffraction (LEED) experiments on the growth-dynamics of oxygen superlattice structures on a W(112) surface,[8] computer simulations on discrete order-parameter models such as the Ising[14,15] and p-state Potts[16] models, and on continuous variable systems as the ϕ^4 model[17] and the nonconserved Ginzburg-Landau model.[18] These studies establish an universality class with $n=\frac{1}{2}$, which is independent of the discrete or continuous character and the degeneracy of the order parameter. Yet, slower growth with $n<\frac{1}{2}$ has been observed in certain anisotropic systems with a continuous order parameter[19] as well as in anisotropic Potts models with large p.[20] Based on such observations, Mouritsen has suggested[21] that it is the potential of the walls to soften in response to the curvature, which leads to a slowing down of the growth rate, and could break down the basic assumptions of the Allen-Cahn theory.[12] This point has been disputed in several works[22,23] arguing that the width of the walls becomes irrelevant when it is much smaller than the radius of curvature. Nevertheless, slow growth is found in simulations and the general reason is not conclusively found.

In the context of this scenario of the universality classes for domain growth, our model for the martensitic transformation is described by continuous variables and a nonconserved order parameter with $p=4$ (or $p=2$) and the model is anisotropic. We find the Allen-Cahn law is fulfilled in the sense that the movement of the boundaries can be described as a curvature-driven process which covers a constant area per unit time. Nonetheless the resulting growth exponent does not fit with the Allen-Cahn exponent $n=\frac{1}{2}$. We find two markedly different regimes in the time evolution of the excess energy which can be fitted to $\delta E(t)\sim t^{-n}$. The first regime, which we do not attribute to a true power-law decay, gives an "apparent" exponent of $n\simeq 0.45$, whereas for later times the evolution slows down with an $n\simeq 0.24$. The regimes are separated by a sharp crossover which is proven not to be due to finite-size effects.

The model has the special feature of simultaneously supporting both "hard" and "soft" walls or boundaries. The domain structure is formed in such a way that broad, curved boundaries are connected by sharp, straight boundaries. The sharp, straight boundaries represent stacking faults of finite extent. At the ends the stacking faults are joined with other stacking faults by broad, curved boundaries. The latter are well described as soliton walls. We can separately follow the movement of both kinds of boundaries and find their behavior remarkably different. The sharp boundary disappears following $t^{-1/2}$ whereas the broad boundary disappears as $t^{-1/4}$. We can show that for the $t^{-1/2}$ process the driving force is contained in the intersection point between the sharp, straight boundary and the broad, boundary. The broad boundary moves with constant velocity inversely proportional to its curvature. This movement covers a constant domain area per unit of time. This feature is also, implicitly, of key importance in the Allen-Cahn theory. However, in their case the curvature changes in time, whereas in our case it remains constant. For the $t^{-1/4}$ process the driving force is contained in the curvature of the broad boundary in agreement with the basic assumptions underlying the Allen-Cahn law. We will show that the tendency to reduce the curvature does not determine the relevant energy for the process because the energy associated to the curvature is negligible relative to the energy stored in the "effective" length which is the projection on the direction perpendicular to the straight boundaries. A measure for this projection is simply the number of solitons forming the broad boundary. This number can only decrease after the sharp, straight boundary has been eliminated and two broad boundaries meet. Consequently, we find that the sharp boundaries (i.e., the stacking faults) can only move when the extent becomes very small. This slows down the growth process and gives the $t^{-1/4}$ behavior.

The plan of the paper is the following. In Sec. II we review the relevant features of the model and describe its characteristics in the context of the present work. Section III is dedicated to the Monte Carlo simulation of the kinetics of domain growth. After a brief description of the numerical procedure in Sec. III A, we describe how the system relaxes to the equilibrium state in Sec. III B. In Sec. III C we present the results obtained from Monte Carlo simulation. In Sec. IV we give an extensive theoretical analysis of the results. In Sec. IV A we use a relaxation model to describe the early times of the process. In Sec. IV B we modelize the domain wall structure by using a soliton-domain-wall model. In Sec. IV C we analyse the scaling behavior of the system. Finally in Sec. V the results are discussed and the conclusions summarized.

II. THE MODEL

In order to study the dynamics of a displacive transition from a bcc to a closed-packed structure (hcp or fcc), it is convenient to represent the atomic motion by a spin located at the average position in the bcc structure. The model thus excludes atomic diffusion which as a characteristic fact is found not to play a role at the martensitic transformation (MT).[1] To simplify further let us consider only a projection on the $(001)_{bcc}$ plane, which we call the xy plane, shown in the lower part of Fig. 1.

The model system then consists of a square array of size N of classical spins. A ferromagnetic order, in the z direction perpendicular to the plane, corresponds to the bcc phase which we have called the square or cubic phase (or simply z phase) and an antiferromagnetic order corresponds to the closed-packed phase, which we have called the triangular phase or closed-packed structure (or simply the $\pm x$ phase). The following Hamiltonian stabilizes the ferromagnetic and antiferromagnetic order according to the relative strength of the Ising interaction K and the

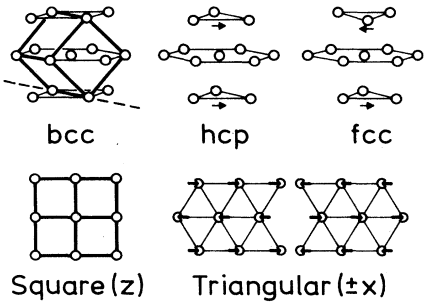

FIG. 1. The upper part shows characteristic three-dimensional parts of the bcc and closed-packed structures. The arrows indicate the direction in which the neighboring planes are displaced under the martensitic transformation. The lower part shows the two-dimensional projection along the bcc [001] direction of this pattern. A spin model representing the atomic displacements, with the spins in the z direction corresponds to the cubic bcc phase (z), and with the spins antiferromagnetically orderd in the xy plane corresponds to the closed-packed hcp phase ($\pm x$). In two dimensions it is natural to refer to these as the square (z) and triangular phases ($\pm x$).

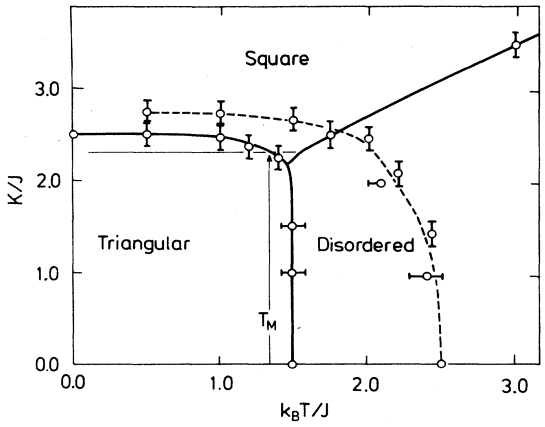

FIG. 2. The calculated phase diagram for the model Hamiltonian [Eq. (1)], solid full line. T_M is the martensitic transition temperature. The dashed phase boundary is calculated for the model with the spins restricted to the upper half of the xz plane, it is of first order. The quenches studies in this paper are performed along the horizontal line at $K/J=2.3$ from high temperatures to $T=0.02J/k_B$.

two-dimensional pseudodipolar interaction J:

$$H=\sum_{\langle i,j\rangle}\{-KS_{iz}S_{jz}+J[\mathbf{S}_i\cdot\mathbf{S}_j-P(\hat{\mathbf{r}}_{ij}\cdot\mathbf{S}_i)(\hat{\mathbf{r}}_{ij}\cdot\mathbf{S}_j)]\}$$
$$-D\sum_i(S_{ix}^4+S_{iy}^4)\ , \qquad (1)$$

where $\hat{\mathbf{r}}_{ij}$ is a unit vector connecting nearest neighbors and we use $P=3$.

The anisotropy term with $D>0$ ($D=2J$), in combination with the dipole interaction, breaks the continuous xy degeneracy and stabilizes at low temperatures an antiferromagnetic order of aligned spins chains in either the x or y direction. This is convenient in computer simulations, since it reduces the number of possible antiferromagnetic domains to four. The number of ferromagnetic domains is two. This model for the MT was introduced previously by Lindgård and Mouritsen[6] and the static properties and the dynamics near such transition temperature discussed for the choice $P=2$ and $p=4$. Here we shall study the nonequilibrium dynamics of the domain formation of ordered regions after a rapid quench from high to low temperature. A preliminary study of this showed that the kinetics was much slower than expected for a curvature-driven growth process.[6,24] The reason for this could be that the interplay between the four kinds of antiferromagnetic domains and the two kinds of ferromagnetic domains creates a number of pinning centers, which effectively hinder the motion of the domain boundaries. Therefore the excess energy stored in the domain boundaries can only very slowly decrease and the system is trapped in a long-lived metastable state. This interesting self-pinning aspect of our model will be discussed in more detail elsewhere.

For $P=2$ the interaction along and between chains is the same and the system exhibits an isotropic domain structure of sharp boundaries with no preferred directions. For $P>2$ the interaction along chains is $(P-1)$ times stronger than between chains. This favors the formation of sharp, straight boundaries between chains (stacking faults) and broad boundaries along the chains (soliton walls via the cubic phase). The interesting aspect of the sharp boundaries, that they can be regarded as stacking faults in the sequence of closed-packed planes, is an essential feature of the martensitic domain structure.[3] For this reason and because of the interesting diversity exhibited by the domain-wall structure, we have chosen $P=3$ for this study.

First, we now simplify the model even further by studying the subspace of the phase space in which only two antiferromagnetic domains and one ferromagnetic domain compete. This is done using the model [Eq. (1)] by restricting the spins to only be allowed to take continuous positions in the upper half of the xz plane. This means a transition between a polarized but disordered $p=1$ state to an ordered $p=2$ state. The results for the full model, i.e., for a disordered or ordered $p=2$ state to an ordered $p=4$ state, will be discussed elsewhere. The phase diagram (Fig. 2) for the full model (solid line) is apart from a simple scaling identical to the one obtained previously[6] for $P=2$. The phase diagram (dashed line) for the restricted model is simpler since there is only a transition between the cubic and the closed-packed phase, but there is no true disordered phase. We can, with this restricted model, study the transition from a high-temperature single-domain cubic phase to the closed-packed phase. We perform temperature quenches along the path indicated, which crosses the first-order transition line between the cubic and closed-packed phases, i.e., the martensitic transformation.

III. KINETICS OF DOMAIN GROWTH

In a typical temperature quench experiment, a system, initially in equilibrium at a temperature T_H, is suddenly

assigned a new lower temperature T_L. Just after the quench, the system is very far from its equilibrium state—which may be an other ordered state—and the question of interest is to investigate how the system relaxes and cools in order to reach the new heat-bath temperature T_L. This is a fundamental problem in statistical mechanics of nonlinear phenomena far from equilibrium, and it is as well of considered practical interest.[25] Theories for situations far from equilibrium are extremely difficult and therefore the Monte Carlo method is a very useful tool to investigate the time evolution.

A. The Monte Carlo numerical procedure

Using Monte Carlo simulation techniques[26,27] we have calculated the time evolution of the domain growth that follows a quench from high temperature to $T \simeq 0$. Our system is a set of N particles arrayed on a two-dimensional square lattice subject to toroidal periodic-boundary conditions. To reduced boundary effects, the main results have been obtained for a large lattice with $N = 200 \times 200$ sites. We also report results for a $N = 100 \times 100$ lattice. The Hamiltonian of the system is given by Eq. (1). The spin variable S_i takes continuous values on the upper-half xz plane, when the z axis is perpendicular to the square lattice. Starting from an initial configuration in which the individual spins are oriented totally randomly in the upper half of the xz plane, the dynamical evolution is described by the optimized spin-flip algorithm described in the Appendix. The unit of time, one Monte Carlo step per particle (MCS), is defined as N attempts to flip individual spins for the system of size N. In order to average over both initial configurations and dynamical evolutions, we have performed several quenches into the triangular phase (the final temperature is $k_B T/J = 0.02$) using different random number sequences.

B. Description of the approach to equilibrium

During the cooling process, it is characteristic that the system evolves through several transient "states" which can grow up and later die, when overtaken by other transient states. A transient "state" is not energetically the most favorable, but is the fastest accessible of a number of states which are energetically more favorable than the state at a given time.

The behavior of our model is illustrated in Fig. 3, where the white areas correspond to the $\pm x$ phase, the grey areas to the z phase, and the transition regions are indicated by the darker regions. The system evolves through the following stages when it is quenched from the highly-disordered, high-temperature cubic state to a very low temperature inside the closed-packed phase region of the phase diagram.

(i) In the matrix of the highly disordered ($\sim$ high-temperature) cubic phase (z), small clusters are nucleated, which are of the highly ordered ($\sim$low-temperature) closed-packed phase of two kinds ($\pm x$) with an even distribution both in number and relative distance. We find in 12 cases of $N = 200 \times 200$ systems an average of 91 ± 2 and 93 ± 2 clusters of, respectively, the x and $-x$ kind, with a mean-square deviation of only 2. The average distance is about 21 lattice spacings. The cluster distribution does not show scaling behavior at this stage with all sizes and distances present at the same time.

(ii) The domains of the z phase also cool down and become well ordered, and simultaneously the $\pm x$ clusters grow and broad, curved domain boundaries are formed.

(iii) The z domains shrink and the domain boundary width is optimized by creating two kinds of connected domain boundaries separating the $\pm x$ domains. A new sharp and *straight boundary* (abbreviated as S boundary) in the x direction emerges and a broad *curved* solitonlike *boundary* (abbreviated as C boundary), predominantly in the y direction, is established. The two kinds of boundaries are illustrated in Fig. 4. The soliton in the C boundary is a soliton in the xz plane but in the figure and all the following displays we have drawn this in the xy plane for illustrative purposes. The sharp S boundary is straight because a curvature (a kink) costs a high energy. In comparison the energy difference between curved and straight C boundaries is negligible. This is the reason for the S boundaries (stacking faults) being straight, but the soliton C boundaries being curved.

(iv) The system now is fully phase separated and consists of only $+x$ and $-x$ domains separated by boun-

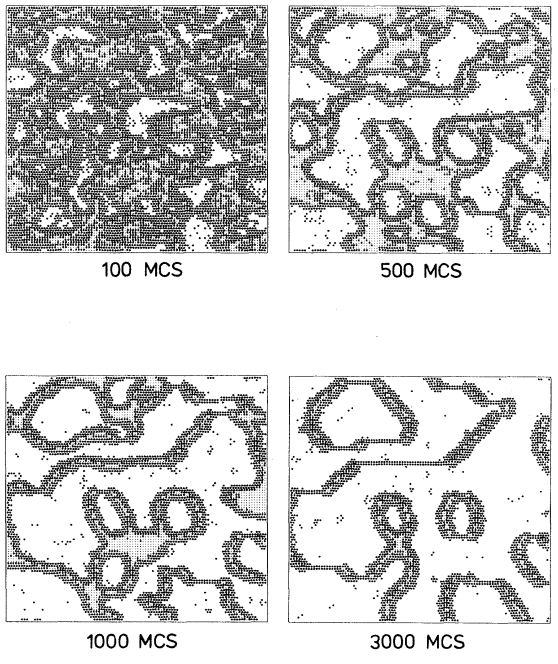

FIG. 3. Snapshots of the evolution of the ordered domains and the domain walls during a quench (we show one quarter of a 200×200 system). The white areas are the $\pm x$ domains, the grey areas the z domains, and the darker regions and single dots disordered spins, drawn as -0 indicating their deviation. At early times $t = 100$ MCS one sees nucleation of $\pm x$ domains in a disordered z matrix, at later $t = 3000$ MCS one sees two kinds of domain walls have evolved; see Fig. 4.

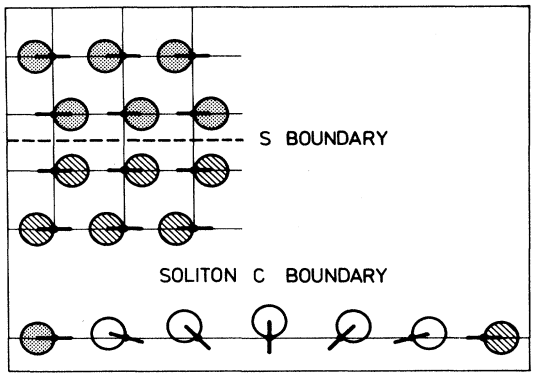

FIG. 4. The upper part shows s sharp S boundary separating $a+x$ (dotted) and $a-x$ (dashed) domain. The circle indicates the displaced atom or the spin, i.e., $-0=\rightarrow$. The lower part shows a broad, solitonlike domain wall, a C-boundary between the $+x$ and $-x$ domains with the atomic displacements in the xz plane. However, for the purpose of illustration we show this displacement in the xy plane for the configurations. A broad C-boundary in Fig. 3 is a sequence of such solitons.

daries of optimized width. The further evolution occurs by minimizing the length of these domain walls. In Fig. 5 we show the phase boundaries after a long time, 42 000 MCS, and the evolution of intermediate times, 3, 6, 12,

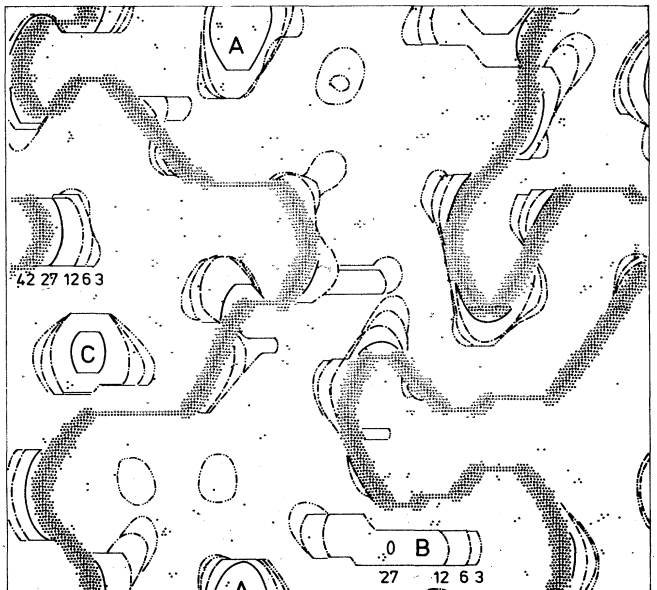

FIG. 5. The configuration of a 200×200 system at very later time $t=42\,000$ MCS. The position of the domain walls at earlier times in units of $\tau=1000$ MCS are indicated ($-\cdots-3\tau$, $-\cdots-6\tau$, $-\cdot-12\tau$, and -27τ, and the actual boundary at 42τ). From this it is possible to follow the domain growth and elimination of smaller features and domains. In particular it is interesting to follow the typical domains indicated by A, B, and C. This is discussed further in Fig. 9.

and 27 (1000 MCS), are indicated by dashed-dotted lines. We notice that the S boundary connecting two C boundaries has to disappear before the C boundaries can be reduced in length.

(v) Finally, for very long times, one might expect that only the C boundaries remain and then the energy is minimized by reducing the curvature. This stage—as a global stage—has not been reached in our Monte Carlo simulations.

Of principal interest is not the topology of a particular case—such as that shown in Fig. 3—but it is the behavior of a thermodynamic ensemble of such cases. To study the approach to equilibrium, several statistical quantities, which could be monitored, have been suggested such as excess energy, domain radius, moments of the structure factor, etc. Let us focus our attention of the excess energy defined as

$$\Delta E(t)=E(t)-E_T(\infty)\ , \tag{2}$$

where $E(t)$ is the nonequilibrium energy at time t. At $t=\infty$ the system is supposed to reach the equilibrium with the energy $E_T(\infty)$, at the temperature T towards which the quench is directed. $\Delta E(t)$ is a good quantity in the sense that is a self-averaging quantity[17] which measures the total nonequilibrium internal energy associated with the entire domain-boundary network. That means it is a measure for the distance to the equilibrium state with the lowest free energy.

We have found that our model system [Eq. (1)] shows a slow decay of $\Delta E(t)\sim t^{-n}$ with $n\simeq\frac{1}{4}$ at later times and a markedly different power law—let us call it—the apparent power law at earlier times. Such a low-temperature behavior for the nonconserved case has been reported earlier[19,20,21] and it was attributed to the presence of soft domain boundaries. Later[17,23] this observation was disputed and it was suggested that a different interpretation of the data could give $n=\frac{1}{2}$ in agreement with the Allen-Cahn theory. In our case it is definitely excluded, in this way, to provide agreement with the Allen-Cahn predictions for the excess energy exponent. In order to gain understanding of the reason for the slow approach to equilibrium, we shall analyze the process in detail, focusing our attention on the mechanism through which it takes place.

C. Monte Carlo results

In this section we present the statistical analysis of the results obtained from Monte Carlo simulation of the quench experiments from a high-temperature cubic phase with $\langle S_z\rangle=0.50$ to a low-temperature closed-packed phase at $T=0.02J/k_B$ with two kinds of domains (see the Appendix). In Sec. IV the interpretation of these results will be discussed in more detail.

Figure 6 shows a log-log plot of the time evolution of the excess energy $\Delta E(t)$ for both $N=100\times100$ and $N=200\times20$ size systems. The number on each curve indicates the best fit to an exponent n for $\Delta E(t)\sim t^{-n}$, corresponding to the slope. Figure 6 shows that for early times a regime, that after a transient, obeys a power-law decay with an exponent of $n_1\sim\frac{1}{2}$. At $t=t^*$ the evolution

crosses over to a slower decay characterized by an exponent of $n_2 \sim \frac{1}{4}$. Both regimes are clearly separated. For the $N = 100 \times 100$ size system $t^* = (2000 \pm 200)$ MCS and for the $N = 200 \times 100$ size system $t^* = (2500 \pm 400)$ MCS. The crossover point does not significantly depend on the size of the system and cannot be attributed to finite-size effects. The sharpness of the crossover shows it is not due to an additional faster decay process with a power law of the type $t^{-1/2}$. This would give a crossover region of several decades in time. Rather, it is indicative of an additional exponentially fast decaying process. The exponent n_1 is therefore an apparent exponent. We have performed 14 quenches for the $N = 100 \times 100$, and three quenches for $N = 200 \times 200$ systems, approaching the equilibrium single-domain state. The exponents and t^* agree within the statistical error bars as indicated in Figs. 6(a) and 6(b).

It is important to distinguish and separately discuss the quenches which do not develop into a single-domain state. For the $N = 200 \times 200$ system we have observed that a very significant fraction of quenches ($\frac{9}{12}$) evolve into two kinds of two-domain "slab" configurations (see Fig. 7) which are long-lived metastable states that can only decay via very unlikely thermal fluctuations. This gives rise to lower apparent exponents in both regimes if $E_T(\infty)$ is simply taken to be the single-domain equilibrium value. These effects are an artifact of the finite-size and periodic-boundary conditions for the system[28] and have been discussed before[29] in the context of domain-growth process. As we will show, it is possible to calculate the final energy of the slab configuration $E_T(\infty)_{\text{slab}}$ when we know the domain-wall energy. In Fig. 6(c) the dashed-dotted lines are the corrected excess energy relative to the slab configuration energy $E_T(\infty)_{\text{slab}}$ for the case of two straight boundaries either along x (—·—·—·) or y (··—··—) directions. In Fig. 7 we show two representative examples of such a configuration: (a) corresponds to a quench which evolves into a S-slab configurations, whereas (b) evolves into a C-slab configuration. Notice that in Fig. 6(c) the correction (·—·—) refers to a perfect S-slab configuration. In the real example [Fig. 7(a)] the boundary will also include some pieces of C boundary and the corrected energy must be placed between the two ideal cases. The conclusion is that after this correction the exponents are in agreement with the $n_1 = \frac{1}{2}$ and $n_2 = \frac{1}{4}$ found for the quenches to the single-domain state. Therefore, all the performed quenches give consistent results, violating the Allen-Cahn law.

At very late times one can in Fig. 6(c) notice another crossover (at $t \sim 20\,000$ MCS) to a faster decay. We suppose this is due to a lack of proper statistical distribution of domain sizes because of the finite-size and periodic-boundary conditions of the system. This is a finite-size crossover effect.

In the lower part of Fig. 8 we have plotted the evolution of the S-boundary-length L_s and the projection of the C boundary length on the y direction, L_c, measured in the number of solitons, and also the number of particles belonging to a z domain (cubic phase). These quantities clearly show a transient state at early times [stage (i) described in Sec. III B, $t \leq 500$ MCS] where the z phase

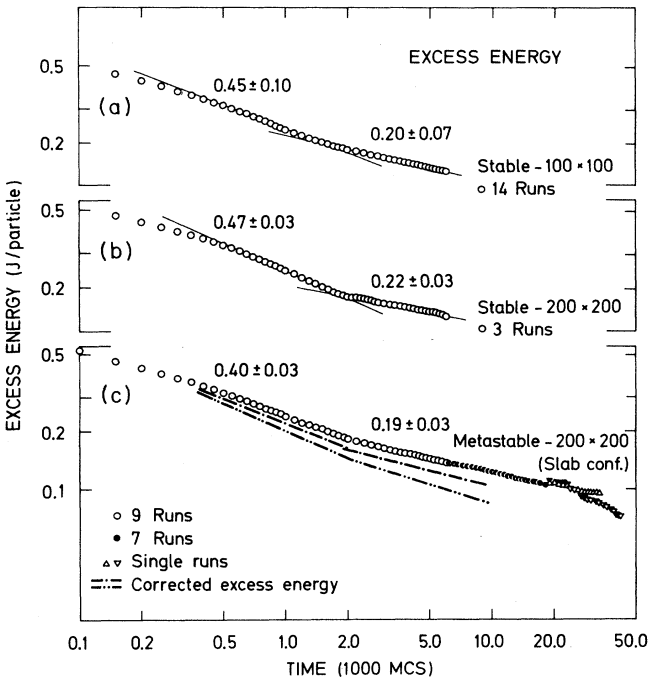

FIG. 6. The average excess energy $\Delta E(t)$ relative to the stable, single-domain ground-state energy $E_T(\infty)$ is plotted for two system sizes (a) 100×100 for 14 runs and (b) 200×200 for three runs. Consistently, an early regime is found with an exponent $n \sim \frac{1}{2}$ and a sharp crossover to a second regime with a smaller exponent in $\sim \frac{1}{4}$; (c) shows the excess energy for nine different 200×200 systems which develop into a metastable slab configuration. The signatures indicate the excess energy relative to $E_T(\infty)$ as above, yielding too low exponents. The excess energy relative to the relevant, higher slab energy $E_T(\infty)_{\text{slab}}$ is between the limits indicated by —·— and —··—. Both exponents and crossover for the corrected excess energy agree with the stable cases (a) and (b). At very later times $t > 25\,000$ MCS finite-size effects are detected for separate runs (∇).

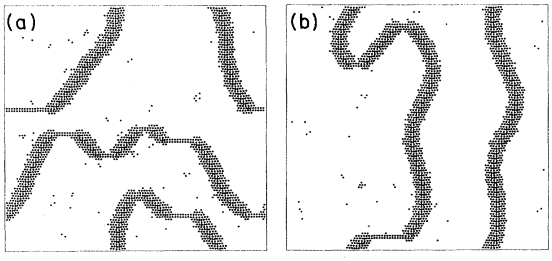

FIG. 7. Two metastable slab configurations for a $N = 100 \times 100$ system, (a) slab in the x direction with the lowest possible energy per particle $(2J)2/\sqrt{N}$, corresponding to two straight S boundaries, (b) slab in the y direction, with lowest energy $(4J)2/\sqrt{N}$, corresponding to two straight broad C boundaries.

grows and very broad domain boundaries separating the $\pm x$ domains are formed. At this stage it is difficult to measure the length of domain boundaries.

At stage (ii), the length of the S boundary increases and at the same time the z domains are being eliminated (the system realizes that the z phase is not optimum). The elimination of the z phase allows to the boundary width to become more narrow and to be optimized. This process is finished at $t^* \simeq 2500$ MCS which corresponds to reaching the maximum of the S-boundary length. For all individual quenches it is found that the crossover time t^* for the exponent coincides with the maximum of L_s and the disappearance of the z domains.

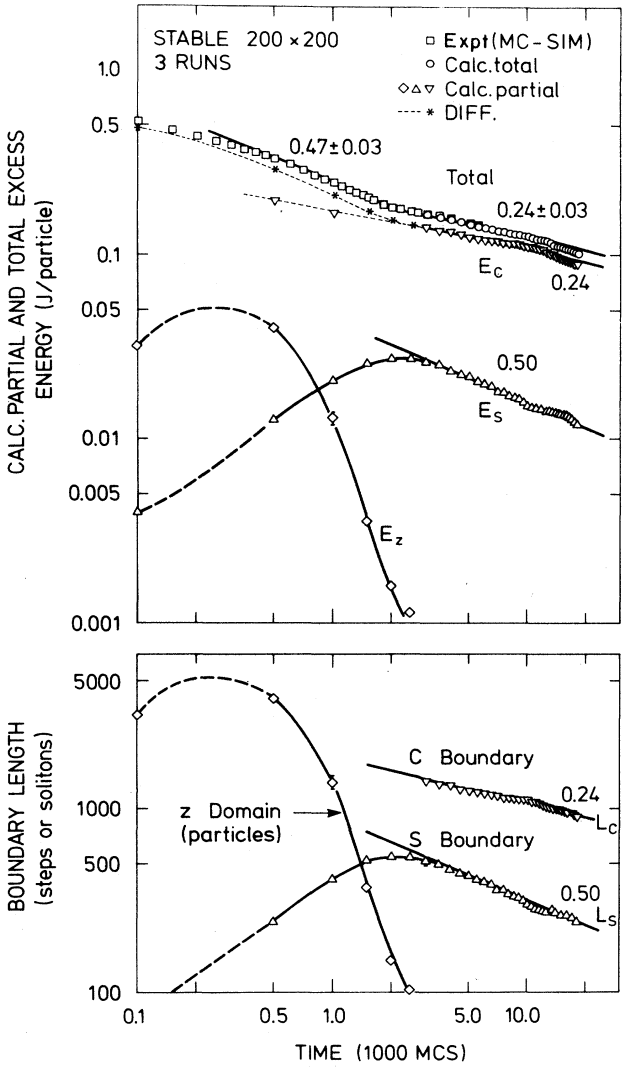

FIG. 8. Analysis of the average properties of the 200×200 systems [Fig. 6(b)]. The lower part shows the counted total number N_z of spins in z domains (larger than three connected z spins), the total length L_s of the S boundary (the number of steps), and the total length L_c of the projection of the C boundary on the y direction, i.e., the number of solitons. Notice the different exponents $n=\frac{1}{2}$ for L_s and $n=\frac{1}{4}$ for L_c. Furthermore, the maximum of L_s and the disappearance of the z domains coincide with the crossover time found in the excess energy show on the upper part ($\Diamond$). The calculated partial contributions E_s, E_c, and E_z due to L_s, L_c, and N_z show first that the calculated total energy ($\circ$) agrees with the simulation ($\Box$) and secondly that E_c is the dominant contribution. The dashed line indicates E_c extrapolated into the first regime. ($- - - *$) is the total energy ($\Box$) minus the contribution from L_s and N_z ($-\nabla$) includes the conversion of C- to S- boundaries. Consequently the maximum in L_s is responsible for the crossover.

After this we reach stage (iii) with a regular pattern of S and C boundaries of optimized with (Fig. 5) with an evolution characterized by a decrease of the length of both boundaries. The decrease follows power laws, but with exponents $n_s=0.50\pm0.03$ and $n_c=0.24\pm0.03$, respectively, for the L_s and L_c lengths.

We can estimate the associated energy quite accurately as follows. The energy of each step of the S boundary is exactly $2J$ and the average energy for each soliton of the C boundary is close to $4J$ as will be justified in Sec. IV. Although L_c is not the real length of the C boundary it gives the correct energy and it is much easier to measure. This neglects insignificant energy changes due to curvature effects. We show in the upper part of Fig. 8 the calculated partial energies E_z ($\Diamond$), E_s ($\triangle$), and E_c (∇), the last only for $t>t^*$ and the total energy calculated as a sum of the partial energies $E_z+E_s+E_c$ ($\circ$) and compare it with the corresponding Monte Carlo result ($\Box$). The agreement is very good, which means that the neglected curvature energy for the C boundary is indeed negligible in the considered time interval. Most importantly we find that the contribution from E_c (∇) is dominant. For $t<t^*$ we can easily define and calculate E_s and E_z but not E_c. However, we can estimate E_c by subtracting E_s+E_z from the total Monte Carlo excess energy. This gives the extrapolated E_c curve ($*$). At early times this value contains extra contributions due to not optimal domain-wall widths. If one, for t close to t^*, assumes that all boundaries are S or optimized C boundaries and that the most horizontal C boundaries become converted into the energetically cheaper S boundaries, we can also calculate the length of the C boundaries for $t \lesssim t^*$. This gives the straight-line extrapolation (∇).

Now let us summarize the main conclusions from Fig. 8: the S-decrease process, during which only the S boundaries decrease, gives a power-law decay of the excess energy $E_s \sim t^{-n_s}$ with $n_s=\frac{1}{2}$ in agreement with the Allen-Cahn law. The C-decrease process, during which only the projection of C-boundary decrease is a slower process, giving $E_e \sim t^{-n_c}$ with $n_c=\frac{1}{4}$. The energy calculated as E_s+E_c and the Monte Carlo result for the total excess energy $\Delta E(t)$ agree for $t>t^*$. The exponent for the total energy of the decay is determined by the dominant energy E_c because the energy of the unit of the C-boundary length, a soliton, has twice the energy of a unit of the S boundary, a step. An interesting fact is that changes of the curvature energy, which are not considered in the definition of L_c, are negligible relative to both E_c and E_s.

We shall now demonstrate that the decrease of L_c is a curvature-driven process and that in both processes the domain area decreases linearly in time. Let us analyze

typical single S-decrease and C-decrease processes. In Fig. 9 we present the time evolution of L_s and L_c for two typical processes involving S- or C-boundary movements, using examples A and B of Fig. 5. Figure 9(a) shows that the single C process (see upper part of the inset) on average follows the square-root behavior expected for a curvature-driven process given $L_c^+ \sim (t_0 - t)^{1/2}$, where it disappears at $t = t_0$. It is important to notice that the decrease in domain area is linear in time and most importantly that two broad boundaries, i.e., L_c^+ can only decrease if they are not separated by any straight boundary. The inset shows the considered domain at the initial time $t \sim 10\,000$ MCS. The length of the lower part L_c^- is prevented from decrease until $t \sim 25\,000$ MCS when the sharp boundary has vanished. The evolution of L_c^+ and that of the lower part L_c^- is then similar. The steps indicate creation of S boundaries which subsequently disappear. Figure 9(b) shows the time evolution of the S-boundary length L_s, in the configuration shown in the inset. This follows a significantly different law. Namely, for each S process $L_s \sim (t_0' - t)$ is linear in time, disappearing at $t = t_0'$. The area change is again linear in time as above. The velocity v of the decrease of L_s depends on the length of the interconnecting broad boundary L_c, but the area change is constant. This indicates that the S-decrease process can as well be considered to be curvature driven.

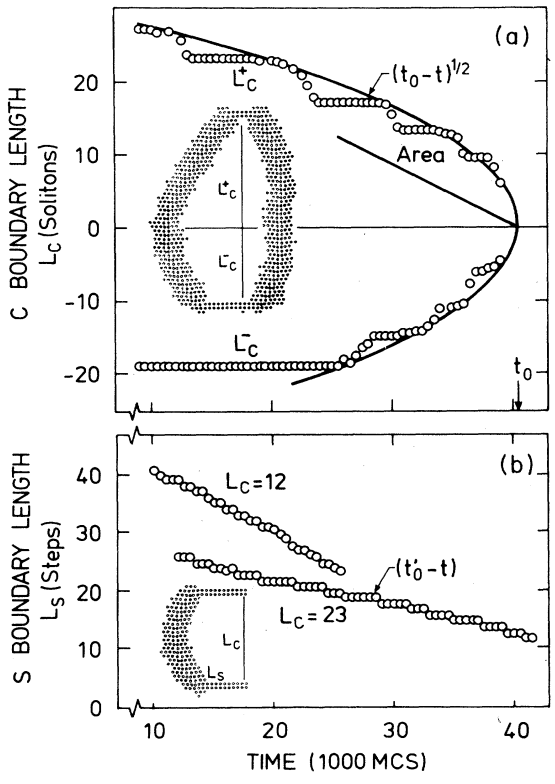

FIG. 9. (a) time evolution of the C-boundary length L_c for the typical case A in Fig. 5 (inset). The upper part L_c^+ decreases as $(t_0 - t)^{1/2}$, whereas the lower part of L_c^- decreases in this way only after the S boundary has disappeared at $t \sim 27\,000$ MCS. The decrease of the area is linear. (b) time evolution of the S-boundary length L_s for the typical case B in Fig. 5 (inset) for two different separations L_c. The area decrease is, again, obviously linear.

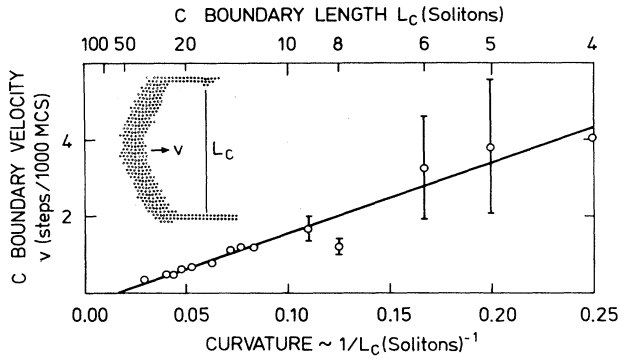

FIG. 10. The speed of C boundary v is a linear function of the inverse length L_c^{-1}. The decrease of the area is linear in time and independent of L_c, in accord with a curvature-driven process.

In Fig. 10, for different values of L_c, we have plotted the velocity v with which L_s decreases when the C boundary moves towards its center of curvature. We accurately find a linear relation between v and L_c^{-1}. Since L_c^{-1} is a direct measure for the curvature of the broad C boundary, this is in agreement with the Allen-Cahn assumption[12] which states that the interfacial velocity is proportional to the curvature. The special feature of the S process is that the velocity is constant in time, since L_c, and thus the curvature, does not change during the process. In fact, a general consequence of the Allen-Cahn assumption is that the decreasing domain area does evolve linear in time. With this formulation, the assumption can be applied even for the special case where the curvature in a given direction is zero, as for the S boundary in our case. As a test of this we have plotted in Fig. 11 the time evolution of the domain area for three different cases, A, B, and C from Fig. 5. In all the cases we find a linear time dependence in agreement with the more general Allen-

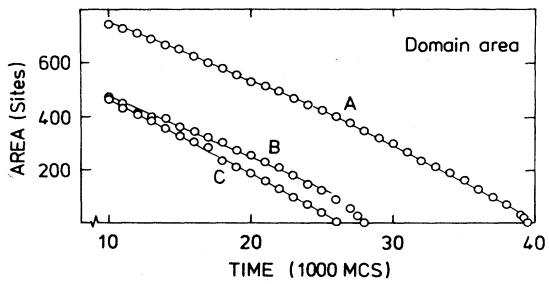

FIG. 11. The decrease in area of the three typical domains A, B, and C in Fig. 5 is approximately linear and the speed (slope) is almost identical for the C decrease (C and A for $t > 25\,000$ MCS and the S decrease (B and A for $t < 25\,000$ MCS), the S decrease being marginally slower.

Cahn assumption.[12] The conclusion from the Monte Carlo simulations is, therefore, that S and C decrease as single processes, follow the basic assumptions of the Allen-Cahn theory in the sense that they are curvature-driven processes, with the domain area decreasing with linear time dependence. For the single processes the time dependences are $L_c \sim (t_0 - t)^{1/2}$ and $L_s \sim (t_0' - t)$. The L_c follows the normal Allen-Cahn behavior and L_s the anomalous, but still Allen-Cahn behavior; namely, for zero curvature.

The global processes, which depend on the statistical distributions of L_s and L_c, give for the excess energy a decrease of $\Delta E_c \sim t^{-1/4}$ and $\Delta E_s \sim t^{-1/2}$. Here the S-decrease process is in agreement with the Allen-Cahn theory in spite of the anomalous single-process behavior. However the C-decrease process violates the Allen-Cahn theory and is much slower, in spite of the fact that the single process obeys normal Allen-Cahn behavior. Finally the total global excess energy follows $\Delta E(t) \sim t^{-1/4}$ because it is dominated by the C-decrease process.

IV. THEORY AND ANALYSIS OF THE APPROACH TO EQUILIBRIUM

In this section we analyze what we have presented in Sec. III. In Sec. III A we used a Langevin equation with a Ginzburg-Landau free energy to theoretically explain the first regime found in the time evolution of the energy. In Sec. III B we explain the relevant features of the domain-wall structure by making use of a soliton-domain-wall model. Finally, in Sec. III C we apply the scaling concepts to our system in order to understand the energy exponents found in our simulations.

A. Relaxational model

The simplest theory for the relaxation in the nonlinear-ordering process is the Ginzburg-Landau theory. This does not consider the domain competition problem at all, but applies for the time dependence of the order parameter. Suppose the free energy is written simply as

$$F = \frac{1}{2\chi_x} M_x^2 + \tfrac{1}{4}\beta M_x^4 + \frac{1}{2\chi_z} M_z^2 + \tfrac{1}{4}\gamma M_z^4 + C \ , \tag{3}$$

where β and γ are constants and C involves a coupling between M_x and M_z and higher-order terms, but it is here neglected for simplicity.

The inverse susceptibilities have the form $1/\chi_\alpha \sim (T - T_c^\alpha)$ and are negative at small T since $T < T_c^x < T_c^z$. The time evolution is given by the Langevin equation

$$\frac{dM_\alpha}{dt} = -\frac{\partial F}{\partial M_\alpha} \ . \tag{4}$$

Using Eq. (3) we find

$$M_\alpha^2(t) = \tfrac{1}{2}\left[1 + \tanh\left[\frac{t}{|\chi_\alpha|}\right]\right] , \tag{5}$$

assuming that at saturation the order parameter is one. In our case, where $T < T_c^x < T_c^z$, we find from Eq. (5) that the z order develops fastest simply because $1/|\chi_z| > 1/|\chi_x|$. This explains the fast evolution of the order in the z matrix in stage (i).

The description of the evolution of the x droplets requires a theory of nucleation, which predicts that droplets above a critical size grow exponentially. Neglecting the domain aspect, how does the system approach the equilibrium value $M_x = M_0 = 1$? Suppose the system (with fluctuations) in a short-time reaches the free energy at $t = 0$ corresponding to $M = M_0/\sqrt{2}$, which still corresponds to a high temperature $\sim 0.9 T_c^x$. The excess Ginzburg-Landau free energy $\Delta F_{\rm GL}$ can then by use of Eqs. (3) and (4) be written as

$$\begin{aligned} \Delta F_{\rm GL} &= F(t) - F(\infty) \\ &= \frac{M_0^2}{16|\chi_x|} \cosh^{-4}\left[\frac{t}{|\chi_x|}\right] . \end{aligned} \tag{6}$$

This is an exponentially fast approach towards a fully ordered single-domain state. However, at later times this is hindered by the competition between equivalent domains and the formation of domain boundaries. Supposing the excess energy due to the boundaries decreases algebraically like $t^{-\alpha}$; then the total excess free energy is

$$\Delta F = \Delta F_{\rm GL} + a t^{-\alpha} \ . \tag{7}$$

The first term represents the optimization of the order inside the domains and of the width of the domain boundaries. This behavior is the one found in stages II and III of Fig. 3. Figure 12 shows that the optimization process terminates abruptly and gives rise to a sharp crossover behavior with an apparent exponent. In contrast, the transition between two algebraic behaviors $\Delta F = a t^{-\alpha} + b t^{-\beta}$ with $\beta = 2\alpha$ would give a very broad crossover, as also shown in Fig. 12. The Ginzburg-

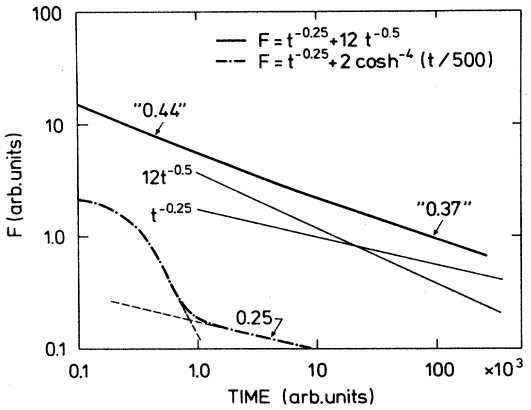

FIG. 12. Example showing that a sum of two algebraic decays (——) exhibits a very broad crossover region and wrong effective exponents. A sharp crossover is provided by a sum of an exponentially fast decaying process and an algebraic decay (—·—). The behavior appears to be algebraic also below the crossover, with an apparent exponent. This is qualitatively the behavior observed in Fig. 6.

Landau theory could be considerably refined by taking into account the competition between the development of z and x order. However it might not be worthwhile since it neglects the domain aspect. Let us now turn to this problem.

B. Soliton domain-wall model

We now discuss the regime where the domains compete and the excess energy is all stored in the domain walls. It is important to estimate the domain-wall energy in order to find the dominant features. We have tested that the domain wall between the two $\pm x$ domains is very accurately described by a soliton function.[30] The π soliton in the x-z plane is given by

$$S_x(\mathbf{r})=\frac{4}{\pi}\tan^{-1}\left[\exp\left[\frac{\pm(\mathbf{r}-\mathbf{r}_0)}{w}\right]\right]-1\ , \tag{8}$$

with $S_z^2(\mathbf{r})=1-[S_x(\mathbf{r})]^2$. Here $\mathbf{r}_0$ indicates the position of the soliton maximum in either the x or y direction in units of the lattice parameter $a=1$ and w is the width of the soliton.

For the domain walls shown in Fig. 4 the S boundary, which we call a step, is a soliton of zero width and a position $\mathbf{r}_0=(0,y_0)$ with an arbitrary y_0 different from zero, but less than 0.5; whereas the C boundary, which we call a soliton, has finite width and it is drawn for the position $\mathbf{r}_0=(x_0,0)$ with $x_0=0$. The domain walls consist of a sequence of such steps or solitons and their energy depends on $\mathbf{r}_0$ and w. The S boundary is straight, but the C boundaries are curved. In the real simulation the broad solitons may accommodate their width and position slightly when they are relatively displaced; this is, however, a small effect and is neglected in the following. The calculated energy surface per soliton or step of the soliton domain walls are shown on Fig. 13 at $T=0$ K as a function of the width and displacement. Figure 13(a) shows the energy surface for a soliton in the x direction $\mathbf{r}=(r,0)$, i.e., along the chains. It has two minima as a function of the width w; one for $w=0$ and one for $w=w_0=0.38a$ corresponding to $\mathbf{r}_0=(x_0,0)=(0,0)$ in Fig. 13(a). During the process of width optimization the initially very broad walls become rapidly more narrow and trapped in the minimum corresponding to w_0. The system remains there at low temperature because it cannot jump across the high barrier which separates it from the minimum with $w=0$. For $w=w_0$ there is only a small preference for the x position of the minimum. This is shown on the projection of the magnitude and position

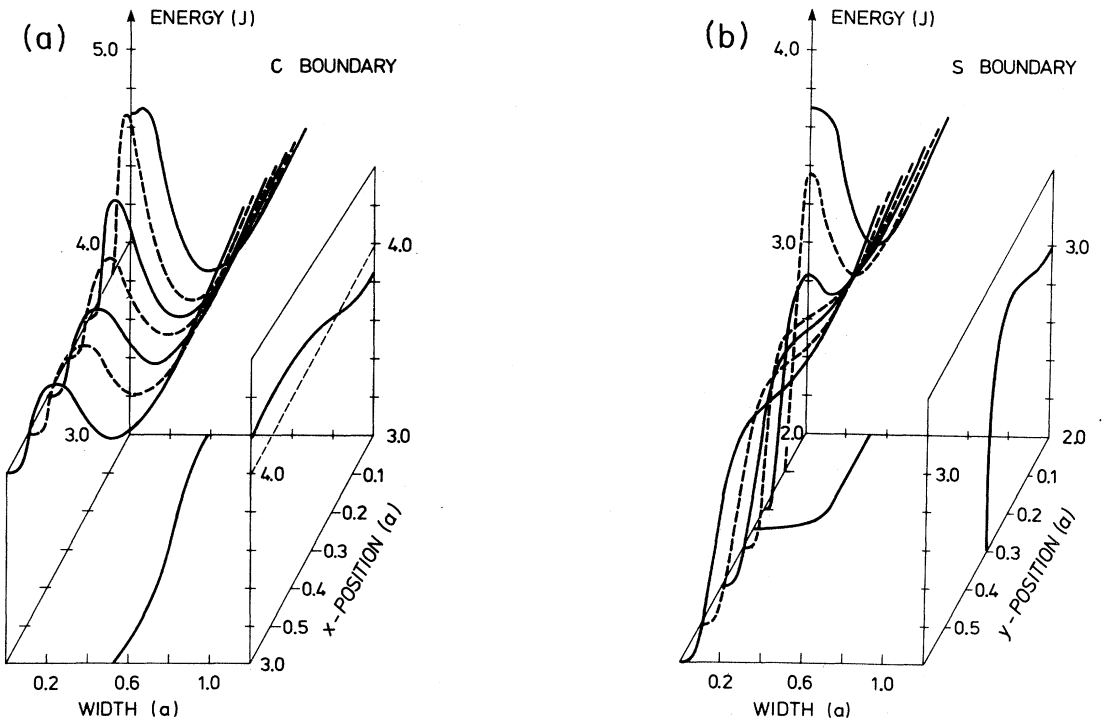

FIG. 13. (a) The energy surface for a π soliton with a width w and the x position x of its maximum between two lattice sites in the x direction (solitons in a C boundary, see Fig. 3). The absolute minimum is $E=3.85J$ for $(x_0,w_0)=(0,0.38a)$. The line in the horizontal plane indicates the projection of the energy minimum, the vertical projection is the corresponding energy. (b) Same for a soliton with a width w and position y in the y direction (solitons in a S boundary; see Fig. 3). Here, there is a narrow valley with a position-independent minimum at $E=2J$ for $w=0$. Notice the large, sharp barrier $E=3.7J$ at $y=0$ for this valley. There is lower energy pass via the local minimum $E=3J$ at $(y_0,w_0)=(0,0.3a)$.

of the energy minimum in the (x,w) plane. The result is, therefore, that a broad C boundary can easily move along the x direction. A typical curved wall will consist of solitons more or less randomly distributed along the (x,w) minimum path and the average energy per soliton is therefore about $4J$. The energy gain for having a straight C wall is only about $0.2J$. Figure 13(b) shows the energy surface for the wall energy for soliton with $\mathbf{r}$ propagating in the y direction, i.e., perpendicular to the chains. The energy surface exhibits again two minima, but now the finite width minimum is a local minimum at $(y,w)=(0,w_0)$ which along the projected minimum path is separated by a tiny energy barrier from the absolute minimum of $E=2J$ at zero width. However, very important is that there is a large barrier at $(y_0,w_0)=(0,0)$ preventing the step from moving in the y direction, also the energy cost of two displaced steps (called a kink) is a very high $4J$. During the width optimization process the system can remain for a short while in the local minimum for $w=0.3$, but it will rapidly find the absolute minimum corresponding to $w=0$. These are the reasons for the S boundary being sharp and straight and further why the sharp S boundary (i.e., at the stacking fault) cannot move in a perpendicular direction. The different behavior for walls breaking chains and walls between chains arises from the anisotropy in model [Eq. (1)] through $P=3$. When $P=2$ the interaction strengths along and between chains are the same giving rise to "sharp" boundaries both between and along the chains. The simple soliton domain wall model therefore explains the two different kinds of boundaries appearing in our Monte Carlo simulations of the [Eq. (1)] model.

Now we want to study the coupling between the sharp S and broad C boundaries. Figure 5 shows that the intersection between boundaries forms an unique angle. Figure 14 shows the energy of the configuration with two sharp S boundaries in opposite directions and a broad straight boundary as a function of the intersection angle φ. The energy of the configuration can decrease by eliminating steps of the S boundary. As the angle increases from $\varphi=0$, the length of the S boundary decreases and therefore the energy E_s decreases, whereas E_c increases in such a way that the total energy, E_s+E_c, exhibits a minimum for a certain angle φ_0 and the configuration is trapped in a local "metastable" state with $\varphi=\varphi_0$. We find that $\varphi_0=33°$ is independent of both boundary lengths L_s and L_c. From our Monte Carlo simulations we evaluate an "experimental" value of $\varphi_0=30°$. We attribute this small difference to the fact that in the model calculation the solitons are rigid, whereas in the simulations they can relax and accommodate to the skew stacking.

The energy per soliton of a C wall as a function of L_c is given at the top (c) of Fig. 15. Next, in Figs. 15(a) and 15(b) we show the coupling of two S boundaries in the same direction with a broad C boundary. In the simplest case (a) the broad straight boundary is chosen to be perpendicular to the S boundary. The energy of such a configuration as a function of L_c is between the continuous lines which correspond to the most favorable solitons [position $\mathbf{r}_0=(0,0)$, width $=0.38a$ and energy $=3.86J$] and the most unfavorable [position $\mathbf{r}_0=(0.5,0)$, width $=0.53a$, and energy $=4.20J$]. The initial decreasing is due to the corner energy, the relative contribution of which decreases as L_c increases. Although this configuration is the optimum from the point of view of the energy, it will be curved when the corners are moving

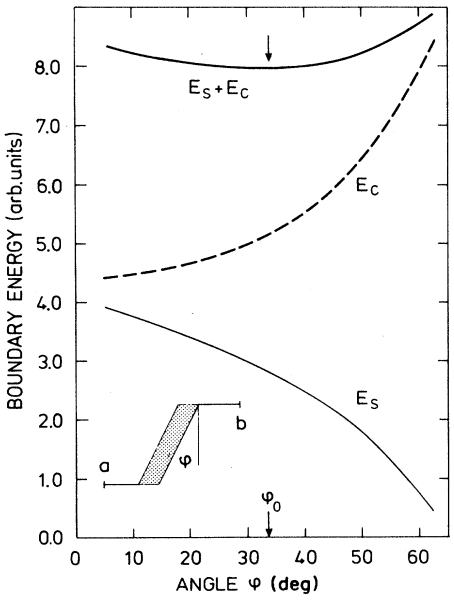

FIG. 14. Boundary energy for a C boundary (of ideal solitons) and two S boundaries in opposite directions (inset) as the function of angle φ. The corners move in opposite directions until the optimum angle $\varphi_0=33°$ is reached.

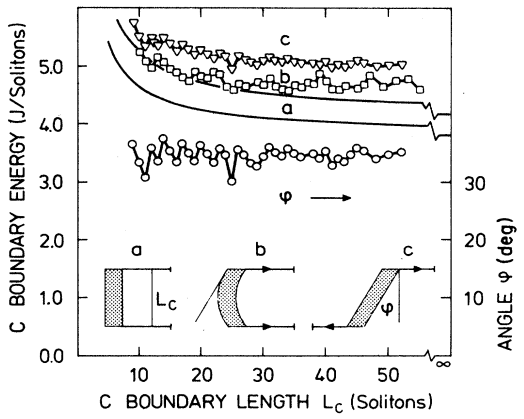

FIG. 15. Boundary and curvature energy. (a) No curvature (——), the difference between the lines indicates energy variation due to the soliton position [see Fig. 13(a)], the increase at small L_c is due to the contribution from the corner energy. (b) Same for a circle-segment-shaped C boundary of ideal solitons. (c) See inset and Fig. 14.

to the right. Figure 15(b) shows the result, assuming the broad C boundary follows a perfect circle segment. The energy of such a configuration gives an asymptotical E_c value of $4.7J$ which is slightly higher than for (a). For each value of L_c the minimum of E_s+E_c determines an optimum radius for the C boundary as well as an optimum angle defined by the tangent to the C boundary in the intersection point. We find that, even though the minimum of E_s+E_c for each L_c determines an optimum radius $R\sim L_c$, the optimum tangential angle $\arcsin(L_c/2R)$ is always the same. One may say the angle determines the radius of curvature. Determined in this way the angle is 45°, which is slightly higher than the one found in the simulation $\varphi=30°$, presumably because of the neglected accommodation effects and furthermore because the curvature of a real case is not exactly a perfect circle segment. If the relaxation of the soliton width and position under the curved condition were taken into account we expect that the relevant absolute energy for a C boundary is close to the average for the minimum path $\sim 4J$ [Fig. 12(a)] as calculated for the single soliton. We use this value for the evaluation of E_c in Fig. 8. The curvature energy can be estimated from the difference between a and b, to be about $0.5J$, which is much smaller than the energy for having a soliton, namely $4J$. This is in agreement with the conclusion drawn from Fig. 8.

C. Scaling behavior

During the growth process, domains of all sizes contribute to the excess energy via their domain walls. Assume for simplicity a two-phase system, where the minority phase, which will disappear, forms only spherical domains. The excess area is the total area of these domains. The Allen-Cahn theory then predicts a decreasing domain radius, R_i, for each domain "i" according to a square-root behavior since the process is assumed to be driven by the curvature, which is inversely proportional to R_i,

$$\frac{dR_i}{dt}\sim-\frac{1}{R_i},\quad R_i(t)\sim\sqrt{t_i-t}\ . \tag{9}$$

The smaller domains disappear first (at $t=t_i$), but an important consequence of [Eq. (9)] is that all domains decrease by the same area per time unit. The system therefore can remain invariant if the area unit A is increasing proportional to the time $A\sim t$ and, consequently, the length unit L increases as $L\sim t^{1/2}$, since $A=L^2$. The excess energy $\Delta E(t)$ for a large distribution of domain sizes is proportional to the total wall length, i.e., $\Delta E(t)\sim\sum_i R_i(t)$. Assuming scale invariance, this length is constant when measured in the time-dependent unit L, i.e., $\sum_i R_i(t)=\text{const}/L\sim t^{1/2}$. From this follows the famous Allen-Cahn exponent $n=\frac{1}{2}$,

$$\Delta E(t)\sim t^{-1/2}\ . \tag{10}$$

For this to hold we need not require pictorial scaling, i.e., self-similarity under magnification as we have in the above simple spherical case. It is clearly sufficient that the excess area distribution is constant when measured in the unit A, which is increasing linearly in time.

Let us now apply the same scaling idea to our results. Consider first the S-decrease process. This is a singular Allen-Cahn situation in which one curvature is zero, namely for the S boundary and for each process "i" the S-boundary length $L_{si}(t)\sim t_i^0-t$ is linear in time and vanishes at t_i^0. This is contrary to the square-root behavior [Eq. (9)]. We found, however, as in the Allen-Cahn theory, that the excess area associated with the S boundary decreases linearly in time [Fig. 9(a)]. The excess energy associated with the S-decrease process is proportional to the total S-boundary length $\Delta E_s(t)\sim\sum_i L_{si}(t)$. Assuming scale invariance with respect to the excess area for S-decrease processes (as above) we find again

$$\Delta E_s(t)\sim t^{-1/2}\ , \tag{11}$$

in agreement both with the Allen-Cahn theory and the computer-simulation results in Fig. 8. In fact this confirms that the area scaling is fulfilled although there is no pictorial scaling (simple magnification). It also proves that the width of the soliton C boundary is not relevant.

Next we consider the movement of the S boundaries (the stacking faults) along the perpendicular y direction thereby giving rise to a C-decrease process. We now must distinguish between two cases. A dormant C-decrease process in which the movement is completely prevented and an active C-decrease process, which we found will start only when the S boundary between two C boundaries has diminished to a length comparable to the lattice distance a, i.e., when the stacking fault has a sufficiently small extent.

Let us first discuss the active C-decrease process. The single process is shown in the upper part of Fig. 9(a), where it is proved to be a standard curvature-driven Allen-Cahn process with the area decreasing linear in time and the linear dimensions in particular L_c decreasing as $\sqrt{t_0-t}$. A new feature is that the excess energy is not proportional to the total boundary length, but is totally dominated by the linear dimension L_c which is the projection along the y direction. This is because one gains $4J$ by removing a soliton, but the curvature energy is only of the order $0.5J$ as illustrated in Fig. 15. The total excess energy for all the active C-decrease processes is then $\Delta E_c^a(t)\sim\sum_i L_{ci}^a(t)$. Assuming as before scale invariance for the area we then find $\Delta E_c^a(t)\sim t^{-1/2}$. The new feature, the dependence only on the projection, can therefore not explain the observed small exponent.

Finally, let us consider the dormant C-decrease process. A single process is shown in the lower part of Fig. 9(a), where it is proved to be dormant until the S boundary disappears at $t\sim 25\,000$ MCS. For a scaling argument for this process we must consider the probability that the intervening S-boundary length L_{si} diminishes to a fixed length of the order of the lattice constant a. When we consider larger and larger scales, the probability P for this to be the case diminishes inversely as the length scale increases as

$$P(L_{si}\sim a)=a/L\sim t^{-1/2}\ . \tag{12}$$

Out of the increasing unit area A, only a fraction A_a of

the area is available for the active C-decrease process

$$A_a = AP(L_{xi} \sim a) \sim tt^{-1/2} = t^{1/2} . \quad (13)$$

The area unit for the subsequent active C-decrease process therefore increases more slowly, and consequently also the corresponding length unit $L_a = A_a^{1/2}$. The decrease in the total excess energy for the dormant C processes, including the subsequent active C processes, is then $\Delta E_c(t) \sim \sum_i L_{ci}(t) = \text{const}/L_a$. We, therefore, find that, because it has to wait for the S boundary to disappear, the dormant C-decrease process gives an excess energy decrease as

$$\Delta E_c(t) \sim t^{-1/4} . \quad (14)$$

This agrees with the observed small exponent. Any active C-decrease process already in operation at early stages will disappear faster than the dormant one, which will dominate the late-time behavior. It is interesting, however, that the equally fast S-decrease process will continue to play an important braking role for the dormant C-decrease process. This is because the prohibitive S-boundary length is to be compared with the atomic scale. The excess energy is dominated by the dormant C process for energy reasons. The slow time evolution with an exponent exactly equal $n = \frac{1}{4}$ is therefore now explained, not as a consequence of the soft boundaries, but as a consequence of a hierarchy of the boundaries, where the decrease of one kind depends on the other. Such an hierarchy is in fact present[23] in the model systems[19,21] in which the slow growth was first discovered. We believe these model systems and our model indeed form a new universality class with $n = \frac{1}{4}$. The growth is, in many respects, in agreement with the Allen-Cahn theory, but it is the special case with zero curvature boundaries. Important examples of such boundaries are stacking faults and twin boundaries in crystals and we expect the class to have many members.

V. DISCUSSION

We have localized and studied a number of crucial aspects determining the kinetics of a quench across a first-order transition line between two ordered structures. Examples could be martensitic transformations, surface rearrangements, or magnetic transitions. We have used a general, yet simple, anisotropic magnetic model with continuous order parameter. This allows a study and a computer simulation of the most important features of a displacive, diffusionless transition—more realistically than the discrete order-parameter models (Potts, ANNNI)—and more economically in computer time than full molecular-dynamics simulations.

A quench from one phase at high temperatures to the low-temperature phase with a number of equivalent domains can be described as follows. As a consequence of the sudden drop in temperature the order parameter of both phases increases exponentially fast according to the susceptibility to form the particular phase. The different domains of the low-temperature phase are nucleated spontaneously and randomly, yet with a very uniform distribution in space. This is important since this distribution determines the domain-boundary network formed after the initial exponential growth is stopped by the competition between domains. The further growth kinetics will now proceed by the decrease of the length of the boundaries. The nature of the boundaries is therefore potentially important for determining growth universality classes. The boundary energy between two crystalline domains will in general depend on the relative orientation of the domains and the orientation of the boundary. The difference in energy of such boundaries is found not to be important. For discrete order parameters the boundaries are always piecewise straight, possibly "curved" with kinks. However, for a continuous order parameter a boundary can both be *continuously curved* or be *straight*. If a kink on a straight boundary is energetically or probabilistically very unfavorable to create we have the interesting situation with a mixture where all boundaries are either perfectly straight or continuously curved. Our model shows this feature. Experimental examples of such straight boundaries are stacking faults or twin faults terminated by smooth, curved boundaries. In agreement with the Allen-Cahn theory the straight boundaries cannot move as there is no driving force. This prevents a decrease of the length and hence of the excess energy stored in the connecting curved boundaries. The straight boundaries represent a kind of time dependent pinning effect, which systematically disappears. This gives rise to a systematically slower decrease of the excess energy t^{-n} with an exponent $n = \frac{1}{4}$ instead of the expected Allen-Cahn exponent $n = \frac{1}{2}$. Our model shows this behavior and led us to define the new universality class with $n = \frac{1}{4}$ first discovered by Mouritsen,[19,21] as a singular limit of the Allen-Cahn theory, namely for the case of mixed boundaries with finite and exactly zero curvature and no kinks. Several different examples of this class have been found in computer simulations, but previously the effect was attributed to some effect of the softness or finite width of the boundaries.[19] This was difficult to understand and much disputed.[22,23] We find that the width is not a crucial feature as such, in agreement with the careful study by Mouritsen and Praestgaard.[21]

However, here we have pointed out that the crucial feature in the models is the pinning effect of straight boundaries and the interrelated decrease of the length of domain boundaries. The effect of this pinning should weaken at higher temperature.[21] We suggest this is due to higher probability for formation of kinks on the straight boundaries (roughening), thereby providing a mechanism for these to move. It is interesting that in the isotropic discrete order parameter models (Ising, Potts) one finds $n = \frac{1}{2}$. This is because in this case there is no interrelation between the boundary movements, which proceed by independent random walks of kinks along the boundaries, and the kinks cannot accumulate themselves in curved boundaries.

We conclude that the growth kinetics for nonconserved order parameter must be subdivided in at least two classes with algebraic time evolution t^{-n} with different exponent $n = \frac{1}{2}$ and $n = \frac{1}{4}$. The first represents independent domain-wall movements, the latter hierarchy

domain-wall movement where the slower domain growth is due to time dependent self-pinning, operative at low temperatures. There are additional features which can slow down the approach to equilibrium even further, experimentally, in particular for $p > d+1$. These are pinning centers, either intrinsic ones formed by the domain boundary network itself, or for the model extrinsic ones formed by impurities, lattice faults or other defects. It is possible one could define a further classification for these cases. We will discuss this further in a subsequent publication.

ACKNOWLEDGMENTS

We thank O. G. Mouritsen for his interest in this study. One of us (T.C.) wishes to thank the Department of Physics of the Risø National Laboratory for hospitality during the time this work was carried out. This work was supported by the European Economic Community (EEC) Stimulation Action, Contract No. ST2-0482.

APPENDIX: FAST MONTE CARLO METHOD FOR STUDYING DOMAIN GROWTH

In this Appendix we describe an optimized efficiency Monte Carlo algorithm for simulating the dynamics of the domain-growth process. It is very time consuming if every spin in the system is being asked to flip in every Monte Carlo step, even a spin well inside an ordered domain where the flip probability is extremely small. We utilized this observation. The method is very close to the original scheme introduced by Metropolis *et al.*,[27] but is optimized to study the late-time stages of the ordering process which follows a deep quench through the transition temperature from $T=\infty$ to a very low temperature.

The dynamics of the model is given by a stochastic interaction with a heat bath via single-site Glauber-type excitation with a probability W_{ij} to change from the state i to the state j. Given the continuous nature of the spin variable S_i we have updated spins sequentially in order to allow spin-wave-type excitations to occur more easily at low temperature. In a standard Metropolis procedure W_{ij} is defined in such a way that a spin i changes depending on the Boltzman factor. That is

$$W_{ij}=\begin{cases} e^{-\Delta E_{ij}/k_B T}, & \Delta E_{ij}>0 \\ 1, & \Delta E_{ij}\le 0 \end{cases},$$

where ΔE_{ij} is the change in energy due to the randomly chosen change of the state of a spin from $S_i \to S_j$. An attempt is accepted when $\Delta E_{ij}<0$. When $\Delta_{ij}\ge 0$ the attempt is accepted only if W_{ij} exceeds a random number between 0 and 1. One Monte Carlo step (MCS)—the unit of time—is then defined as N attempts to change the state of all N individual spins. After the domain structure is formed, we have tested that for a spin *well* inside a domain the probability for an accepted change of state is only 1%. To utilize this we proceed in the following way. Only for one MCS out of 100 MCS, we ask and update all spins with the standard Metropolis procedure described above, whereas during the other 99 MCS we will visit all the spins but ask and update only those found to be in a disordered surrounding, called nonordered spins. This allows us to keep the same definition for the unit of time MCS. All such nonordered spins are plotted in the figures (3, 5, 7, 9, 10) of the configurations. They are those close to a boundary, those having an x component $|S_x|<1-\Delta$, and also those for which the four neighbors are slightly disordered so that $\sum_i |S_{xi}|<4-3\Delta$, here Δ is a parameter measuring the deviation of the order parameter $\langle S_x(T)\rangle$ from the saturation value $\langle S_x(T=0)\rangle=1$.

We call this method a "deviating-spins-algorithm" (DSA) and it is at least twice as fast as standard Metropolis algorithm, yet having the same Monte Carlo time unit (MCS). We have performed several test runs using the full Hamiltonian [Eq. (1)] and the results are shown in Fig. 16. In all the cases the evolution starts from the same random, disordered configuration.

The cases are the following: (a) Metropolis, corresponding to asking sequentially all the particles and updating them according to the standard Metropolis scheme; (b) Metropolis, all particles corresponding to the case (a), but the random number generator is called every time even when not used for $\Delta E_{ij}<0$. Therefore, the used sequence of random numbers is different from the previous case (a). This is done to assure strict comparison with the following fast DSA method. In case (c) the same initial random configuration evolves according to the deviating-spin-algorithm and with exactly the same sequence of random numbers as used in case (b). We have plotted these three evolutions until 2000 MCS.

Any difference between (b) and (c) is then due to the optimization of the updating process. The difference between (a) and (b) is due to the different sequence of random numbers for the standard Metropolis algorithm. In all the cases the agreement is very good. There is no systematic deviation between the fast DSA and the full updating method. Furthermore the maximum deviation observed between them is smaller than the spread found using different random numbers for the standard Metropo-

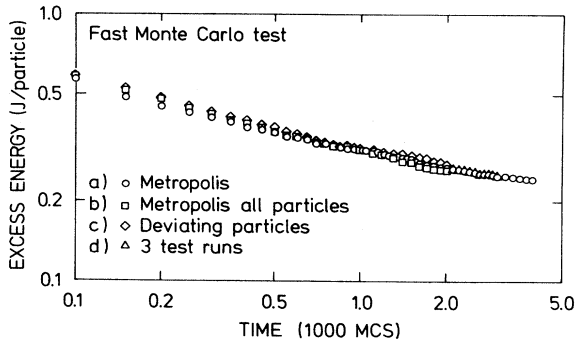

FIG. 16. Monte Carlo calculation of the excess energy using different algorithms as indicated, see text. ◇ and △ represent results of the fast deviating-spins algorithm, compared with the standard Metropolis algorithm ◇ and ○.

lis algorithm. We have analyzed the effect on the evolution of the choice of the Δ parameter, which defines the nonordered spins. In case (d) for $t > 2000$ MCS the deviating-spins algorithm is tested to be identical for three slightly different values of the Δ parameter $\Delta = 0.015$, $\Delta = 0.017$, and $\Delta = 0.020$, starting from the (b) configuration at $t = 2000$ MCS. We compare these runs (Δ) with the standard metropolis algorithm ($\circ$). The agreement is very good. We have in this study always used the value $\Delta = 0.015$.

From this test we conclude that the deviating-spins algorithm does not introduce any systematic change in the evolution and can be used to reach very late stages in the evolution of the domain-growth process costing less than a half of the computer time required for the standard Metropolis algorithm.

---

*Permanent address: Departament d'Estructura i Constituents de la Matèria, Facultat de Física, Universitat de Barcelona, Diagonal 647, E-08028 Barcelona, Spain.

[1]Z. Nishiyana, *Martensitic Transformations* (Academic, New York, 1978).

[2]R. J. Gooding and J. A. Krumhansl, Phys. Rev. B **38**, 1695 (1988).

[3]J. W. Christian, *The Theory of Transformation in Metals and Alloys* (Pergamon, New York, 1965).

[4]V. I. Syntkino and E. S. Yakovleva, Phys. Status Solidi **21**, 465 (1967).

[5]M. E. Fisher and W. Selke, Phys. Rev. Lett. **20**, 257 (1979); D. de Fontaine and J. Kulik, Acta Metall. **33**, 145 (1985). For a review see, *Phase Transformations in Solids,* edited by T. Tsakalakos (North-Holland, Amsterdam, 1983); *Modulated Structures,* edited by T. Tsakalakos (Nijhoff, Amsterdam, 1984).

[6]S. Wen, J. W. Morris, and A. G. Khachaturyan, Proceedings of the International Conference on Martensitic Transformations, Cambridge, Mass., 1979 (unpublished), p. 94; A. G. Khachaturyan, *Theory of Structural Transformations in Solids* (Wiley, New York, 1983).

[7]P.-A. Lindgård and O. G. Mouritsen, Phys. Rev. Lett. **57**, 2458 (1986).

[8]P. S. Sahni and J. D. Gunton, Phys. Rev. Lett. **47**, 1754 (1981); G. C. Wang and T. M. Lu, *ibid.* **50**, 2014 (1983).

[9]T. Hashimoto, T. Miyoshi, and H. Ohtsuke, Phys. Rev. B **13**, 1119 (1976).

[10]*Proceedings of the Physical Properties and Thermodynamic Behavior of Minerals,* Vol. 225 of *NATO Advanced Study Institute, Series C,* edited by E. Sajle (Kluwer Academic, New York, 1988).

[11]J. D. Gunton, M. San Miguel, and P. S. Sahni, in *Phase Transitions and Critical Phenomena,* edited by C. Domb and J. L. Lebowitz (Academic, New York, 1983).

[12]S. M. Allen and J. W. Cahn, Acta Metall. **27**, 1085 (1979).

[13]I. M. Lifshitz, Zh. Eksp. Teor. Fiz. **42**, 1354 (1962) [Sov. Phys.—JETP **15**, 539 (1962)].

[14]M. K. Phani, J. L. Lebowitz, M. M. Kalos, and O. Penrose, Phys. Rev. Lett. **45**, 3666 (1980).

[15]K. Kaski, M. C. Yalahik, J. D. Gunton, and P. S. Sahni, Phys. Rev. B **28**, 5263 (1983).

[16]G. S. Grest, M. P. Anderson, and D. J. Srolovitz, Phys. Rev. B **38**, 4752 (1988).

[17]A. Milchev, K. Binder, and D. W. Heermann, Z. Phys. B **63**, 521 (1986).

[18]O. T. Valls and G. F. Mazenko, Phys. Rev. B **34**, 7941 (1986).

[19]O. G. Mouritsen, Phys. Rev. B **28**, 3150 (1983); Phys. Rev. Lett. **56**, 850 (1986); Phys. Rev. B **31**, 2613 (1985).

[20]G. S. Grest, D. J. Srolovitz, and M. P. Anderson, Phys. Rev. Lett. **52**, 1321 (1984).

[21]O. G. Mouritsen and E. Praestgaard, Phys. Rev. B **38**, 2703 (1988).

[22]K. Kaski, S. Kumar, J. D. Gunton, and P. A. Rikvold, Phys. Rev. B **29**, 4420 (1984).

[23]W. van Saarloos and M. Grant, Phys. Rev. B **37**, 2274 (1988).

[24]P.-A. Lindgård and O. G. Mouritsen (unpublished).

[25]T. Tasaku, T. Miyoshi, and H. Ohtsuka, Phys. Rev. B **13**, 1119 (1976); T. Hashinoto, K. Mishimura, and Y. Takeuchi, Phys. Lett. A **65**, 250 (1978).

[26]O. G. Mouritsen, in *Computer Studies of Phase Transitions and Critical Phenomena* (Springer, Heidelberg, 1984).

[27]K. Binder, in *Monte Carlo Methods in Statistical Physics* (Springer, Heidelberg, 1979); *Applications of Monte Carlo Method in Statistical Physics* (Springer, Heidelberg, 1984).

[28]E. T. Gawlinski, M. Grant, J. D. Gunton, and K. Kaski, Phys. Rev. B **31**, 281 (1985).

[29]P. S. Sahni, G. Dee, J. Gunton, M. Phani, J. L. Lebowitz, and M. Kalos, Phys. Rev. B **24**, 410 (1981).

[30]For a review of solitons in condensed matter, see A. R. Bishop, J. A. Krumhansl, and S. E. Trullinger, Physica D **1**, 1 (1980).